

Dissecting Quantum Phase Transition in the Transverse Ising Model

Yun-Tong Yang^{1,2} and Hong-Gang Luo^{1,2,3,*}

¹*School of Physical Science and Technology, Lanzhou University, Lanzhou 730000, China*

²*Lanzhou Center for Theoretical Physics & Key Laboratory of Theoretical Physics of Gansu Province, Lanzhou University, Lanzhou 730000, China*

³*Beijing Computational Science Research Center, Beijing 100084, China*

Irrespective of the fact that a complete theoretical description of critical phenomena in connection with phase transition has been well-established through the renormalization group formalism, the understanding of the phase transition itself remains incomplete. For example, the questions like why and how the phase transition happens are still unclear. Here we provide a pattern picture to dissect the quantum phase transition occurring in the transverse Ising model for a finite lattice. After the validity of the pattern formulation obtained is confirmed, the energy contributions of different patterns to the ground state energy provide a sufficient detail to show why and how the phase transition takes place. Furthermore, a histogram of patterns' occupancy calculated by the projections of ground state wavefunction on the patterns also shows the detailed process of the phase transition. Our results are not only fundamental in understanding the mechanism of phase transition, but also of practical interest in quantum simulation platforms.

Introduction.—The investigations of phase and phase transition of matter in nature or laboratory are one of central issues in modern physics, specially in condensed matter physics, statistical physics as well as complex systems by various ways ranging from theoretical models, experimental measurements, numerical methods to quantum simulations. Conceptually, the order parameter and associated symmetry breaking are the foundation to understand and/or describe the process of phase transitions [1, 2], and methodologically the renormalization group built by Wilson in 1970's [3] provides a complete theoretical description of the critical phenomena to occur in the vicinity of the phase transition points.

What are the most important properties of the critical phenomena are so-called universality and scaling behaviors, which classify the phase transitions by critical exponents [4], irrespective of the details of Hamiltonian of systems. Thus it is commonly believed that the critical phenomena in connection with phase transition have been sufficiently described. However, the understanding of the phase transition itself, both thermodynamically and quantum mechanically, remains incomplete [5]. While most of the existing literature focus on the classification of different types of phase transition in various physical systems, few works put emphasis on the mechanism or nature of phase transition or related issues. It should be pointed out that Lee and Yang [6] developed a theory of equations of state and thermodynamic phase transitions, which relates the zeros of the grand canonical partition function in the complex fugacity plane to non-analyticities of the corresponding thermodynamic function. However, sufficient or necessary conditions for the occurrence of a phase transition, to a large extent, remains to be explored [5].

On the other hand, the process of phase transition such as how to break symmetry as the phase transition takes place has been acknowledged by the Kibble-Zurek mech-

anism [7–9], from which two key features describing the process of phase transition have been identified, namely, the critical slowing down and the growth of the correlation length. The properties of the post-transition broken symmetry state can be inferred from such a dynamical process. While the Kibble-Zurek mechanism has been widely tested in various systems [10–15], both experimentally and numerically, its validity and/or applied ranges still remain to be clarified [16].

In this work we present a pattern picture [17] to explore the process of phase transition by taking the prototypical model, namely, the one-dimensional transverse-field Ising model as an example, which is not only of theoretical interest [18, 19], but also has been realized in realistic materials [20, 21]. More importantly, some well-known or unknown physics involved in such a simple model can be simulated or unveiled by various quantum spin simulators [22–28]. It is well-known that this model exhibits a quantum phase transition (QPT) from the paramagnetic (disordered) phase at weak Ising interacting strength to the ferromagnetic (ordered) phase at strong interaction for a given transverse field, even for small simulating systems. For example, onset of a QPT has been observed by using nine trapped ions quantum simulator [23, 24], and the ground state of an artificial Ising spin system comprising an array of eight superconducting flux quantum bits has been obtained by using quantum annealing [25]. Here our aim is to explore the mechanism of the phase transition.

The method we adopt consists of two successive diagonalizations to treat the model with a finite lattice size. The first diagonalization is performed in an operator space to obtain fundamental patterns, characterized by the patterns' energies and the ordered lattice operators. This pattern picture is proved to be equivalent to the original Hamiltonian in nature. The second diagonalization is performed in the usual spin basis, as done

in direct numerical exact diagonalization, which proves the validity of our pattern formulation. With the patterns at hand, we analyze the process of phase transition and identify the roles played by the patterns as varying the Ising interacting strength. This is what means in the title that we dissect the QPT of the transverse-field Ising model. In addition, we present a histogram of pattern occupancy to further show how happens the phase transition underlying the pattern picture. It is straightforward to extend the pattern formulation to higher dimensional cases and other many-body models in order to further explore the intriguing physics of phase transitions involved in those models.

Model and Method.—The Hamiltonian of the quantum Ising model with transverse field reads

$$\hat{H}' = -J' \sum_{i,\delta} \hat{\sigma}_i^z \hat{\sigma}_{i+\delta}^z - g \sum_i \hat{\sigma}_i^x, \quad (1)$$

where J' and g are the Ising interaction between two spins denoting by Pauli matrix $\hat{\sigma}$ located at site i and its nearest neighbors $i + \delta$ and transverse fields, respectively. They are assumed to be greater than or equal to zero, and in this case the Ising interaction is ferromagnetic. For convenience, we reformulate Eq. (1) as $\hat{H}' = \frac{g}{2} \hat{H}$, which means that in the following formalism we take g as the units of energy, and thus one has

$$\hat{H} = -J \sum_{i,\delta} (\hat{\sigma}_i^z \hat{\sigma}_{i+\delta}^z + \hat{\sigma}_{i+\delta}^z \hat{\sigma}_i^z) - 2 \sum_i \hat{\sigma}_i^x, \quad (2)$$

where $J = J'/g$. For simplicity, we limit ourselves to the one-dimensional case, though it is straightforward to extend to the high-dimensional situations. For the chain length L with periodic boundary condition, the model Hamiltonian can be reformulated as

$$\hat{H} = \begin{pmatrix} -i\hat{\sigma}_1^y & \hat{\sigma}_1^z & -i\hat{\sigma}_2^y & \hat{\sigma}_2^z & \cdots & -i\hat{\sigma}_L^y & \hat{\sigma}_L^z \end{pmatrix} \times \begin{pmatrix} 0 & -1 & 0 & 0 & \cdots & 0 & 0 \\ -1 & 0 & 0 & -J & \cdots & 0 & -J \\ 0 & 0 & 0 & -1 & \cdots & 0 & 0 \\ 0 & -J & -1 & 0 & \cdots & 0 & 0 \\ \vdots & \vdots & \vdots & \vdots & \ddots & \vdots & \vdots \\ 0 & 0 & 0 & 0 & \cdots & 0 & -1 \\ 0 & -J & 0 & 0 & \cdots & -1 & 0 \end{pmatrix} \begin{pmatrix} i\hat{\sigma}_1^y \\ \hat{\sigma}_1^z \\ i\hat{\sigma}_2^y \\ \hat{\sigma}_2^z \\ \vdots \\ i\hat{\sigma}_L^y \\ \hat{\sigma}_L^z \end{pmatrix}, \quad (3)$$

where the identity of Pauli matrices $\hat{\sigma}^y \hat{\sigma}^z = i\hat{\sigma}^x$ has been used for each site i and the matrix in Eq. (3) has dimension $2L \times 2L$. It can be diagonalized to obtain eigenvalues and corresponding eigenfunctions $\{\lambda_n, u_n\}$ ($n = 1, 2, \dots, 2L$). We call them in the following patterns marked by λ_n . With these patterns at hand, the Ising Hamiltonian is rewritten as

$$\hat{H} = \sum_{n=1}^{2L} \lambda_n \hat{A}_n^\dagger \hat{A}_n, \quad (4)$$

Pattern λ_1	(-, -)	(-, -)	(-, -)	(-, -)	(-, -)	(-, -)	(-, -)	(-, -)
Pattern λ_2, λ_3	(-, -)	(-, -)	(-, -)	(-, -)	(+, +)	(+, +)	(+, +)	(+, +)
Pattern λ_4, λ_5	(-, -)	(-, -)	(+, +)	(+, +)	(-, -)	(-, -)	(+, +)	(+, +)
Pattern λ_6, λ_7	(+, +)	(-, -)	(-, -)	(+, +)	(-, -)	(+, +)	(+, +)	(-, -)
Pattern λ_8	(-, -)	(+, +)	(-, -)	(+, +)	(-, -)	(+, +)	(-, -)	(+, +)
Pattern λ_9	(-, +)	(-, +)	(-, +)	(-, +)	(-, +)	(-, +)	(-, +)	(-, +)
Pattern $\lambda_{10}, \lambda_{11}$	(-, +)	(-, +)	(-, +)	(-, +)	(+, -)	(+, -)	(+, -)	(+, -)
Pattern $\lambda_{12}, \lambda_{13}$	(-, +)	(-, +)	(+, -)	(+, -)	(-, +)	(-, +)	(+, -)	(+, -)
Pattern $\lambda_{14}, \lambda_{15}$	(+, -)	(-, +)	(-, +)	(+, -)	(-, +)	(-, +)	(+, -)	(-, +)
Pattern λ_{16}	(+, -)	(-, +)	(+, -)	(-, +)	(+, -)	(-, +)	(+, -)	(-, +)

FIG. 1. The patterns and their relative phases obtained by the first diagonalization, marked by the single-body operators $\hat{A}_n = \sum_{i=1}^L [u_{n,2i-1}(i\hat{\sigma}_i^y) + u_{n,2i}\hat{\sigma}_i^z]$ with (\pm, \pm) denoting the signs of $(u_{n,2i-1}, u_{n,2i})$ in the absence of longitudinal field for the one-dimensional transverse quantum Ising model with $L = 8$ under the periodic boundary condition. All patterns are divided into two groups marked by the red and blue frames with $\lambda_n < 0$ and $\lambda_n > 0$, respectively. Moreover, it is noted that $\lambda_n = -\lambda_{2L-n+1}$ (see, Fig.2 (a)). The characteristic difference between these two groups is that for the pattern with $\lambda_n < 0$ (red frame) the operators within the sites are in-phase, but for the pattern with $\lambda_n > 0$ (blue frame) they are out-of-phase. Both these two groups of patterns, different patterns are distinguished by the phases between nearest neighbor sites, which form domains if they are in-phase for $\hat{\sigma}_i^z$, otherwise, kinks if they are out-of-phase for $\hat{\sigma}_i^z$. These patterns obviously correspond to possible ground state or different excitations in the language of particles.

where each pattern λ_n composes of single-body operators

$$\hat{A}_n = \sum_{i=1}^L [u_{n,2i-1}(i\hat{\sigma}_i^y) + u_{n,2i}\hat{\sigma}_i^z]. \quad (5)$$

The validity of Hamiltonian Eq. (4) can be confirmed by inserting into the complete basis $|\{\sigma_i^z\}\rangle (i = 1, 2, \dots, L)$ with $\hat{\sigma}_i^z |\{\sigma_i^z\}\rangle = \pm_i |\{\sigma_i^z\}\rangle$ (see below).

Patterns and Solution.—Before confirming the validity of Eq. (4), we firstly explore the properties of the patterns marked by the single-body operators \hat{A}_n involving the eigenfunctions u_n 's, shown as patterns in Fig. 1 and their amplitudes varying with the interaction strengths in Fig. 2 for $L = 8$. According to the signs of the eigenvalues shown in Fig. 2 (a), all patterns can be divided into two groups, one has negative eigenvalues $\lambda_n < 0$, as marked by red dashed frame, and the other has positive eigenvalues marked by blue dashed frame. There are $L = 8$ pairs of signatures (plus and minus) for each pattern λ_n , which denote the relative phase of the eigenfunctions $u_{n,2i-1}$ and $u_{n,2i}$. It is quite interesting to see

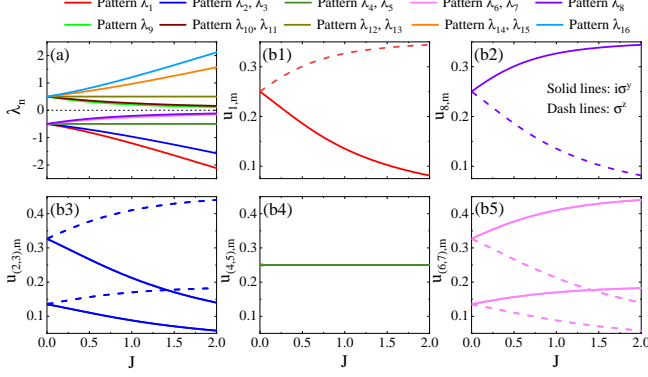


FIG. 2. (a) The eigenenergies of the patterns (colored solid lines) and (b) their eigenfunctions (colored solid lines for the $i\hat{\sigma}^y$ components and colored dash lines for the $\hat{\sigma}^z$ components) as functions of the Ising interacting strength J for $L = 8$. The patterns are divided into two groups (degenerate at $J = 0$), which have positive and negative eigenenergies, respectively, satisfying with $\lambda_n = -\lambda_{2L-n+1}$ ($n = 1, 2, \dots, 2L$). There are still degenerate for the patterns $\lambda_{2,3}$, $\lambda_{4,5}$, $\lambda_{6,7}$, and their positive eigenenergy counterparts. The eigenfunctions of the patterns $\lambda_1, \dots, \lambda_8$ shown in (b) describe the weight changes of the $i\hat{\sigma}^y$ and $\hat{\sigma}^z$ in each pattern with components $u_{n,m}$ (n denotes the pattern number and m its lattice components). It is noted that the patterns $\lambda_{4,5}$ have a constant eigenenergy and constant eigenfunction components, as shown in (a) and (b4), respectively. The corresponding eigenfunctions for the patterns $\lambda_9, \dots, \lambda_{16}$ (not shown here) are in the opposite to their negative counterparts. Here it should be mentioned that the eigenfunctions are free of a total phase factor $e^{i\pi}$ but their relative phases remain fixed.

a few characteristic features for these relative phases in the patterns obtained: (i) for all patterns with $\lambda_n < 0$, the $u_{n,2i-1}$ and $u_{n,2i}$ have the same signs, namely, the wavefunctions (coefficients of operators) for each site are in-phase; on the contrary, they have opposite signs for the patterns $\lambda_n > 0$, that is to say, they are out-of-phase; (ii) for the pattern $\lambda_n < 0$, the pattern λ_1 has only a domain, namely, all sites have the same phase, a typical character of a ferromagnetic order, as shown below, it dominates over all other patterns in the ferromagnetic phase (or strong interaction regime in our presentation); (iii) from the pattern $\lambda_{2,3}$ to λ_8 , the number of domains reads 2, 4, 6, and 8, which corresponds successively to the excitations of 2, 4, 6, and 8 kinks, with possible different orders of the kinks in degenerate cases such as the patterns $\lambda_{2,3}$, $\lambda_{4,5}$, and $\lambda_{6,7}$; (iv) in the pattern λ_8 , the phase is opposite for each pairs of nearest neighbor sites, which corresponds to the opposite limit of the pattern λ_1 ; (v) similar behaviors of the phases in the patterns $\lambda_n > 0$ have also been observed in the lower blue frame.

After clarifying the pattern picture obtained, we solve Eq. (4) by inserting into the complete basis, as mentioned above. Firstly, one readily obtains the matrix

$[\hat{A}_n]_{\{\sigma_i^z\}, \{\sigma_i^z\}'} = \langle \{\sigma_i^z\} | \hat{A}_n | \{\sigma_i^z\}' \rangle$ and then Eq. (4) can be solved by diagonalizing the matrix with elements

$$\langle \{\sigma_i^z\} | \hat{H} | \{\sigma_i^z\}' \rangle = \sum_{n=1}^{2L} \lambda_n \times \sum_{\{\sigma_i^z\}''} [\hat{A}_n^\dagger]_{\{\sigma_i^z\}, \{\sigma_i^z\}''} [\hat{A}_n]_{\{\sigma_i^z\}'', \{\sigma_i^z\}'}. \quad (6)$$

Figure 3 (a1) & (b1) present the results for the ground state and the first excited state as functions of the Ising interaction J , respectively, for $L = 8$, as shown by heavy black solid lines. In order to confirm the validity of the pattern formulation, the results of direct exact diagonalization have also presented for comparison, shown as circles. The exact agreement between them from weak to strong interaction regimes is noticed, which is not surprising since no any approximation has been introduced.

The nature of phase transition.—It is well-known, as also mentioned above, that the one-dimensional transverse Ising model exhibits a QPT from ferromagnetic phase to paramagnetic phase at critical transverse field g_c [18] for the ground state at zero temperature. Since here we take the units of energy scaled by the transverse field g and thus it happens around $J = J_c = \frac{1}{2}$ for the one-dimensional case. For weak interaction regime ($J < \frac{1}{2}$) the system is in the paramagnetic phase and in the opposite side, the regime with $J > \frac{1}{2}$ is called the strong interaction one, which roughly correspond to the weak and strong coupling regimes, respectively, in the quantum Rabi model [17, 29].

For the QPT presented here, it happens as the first excited state and the ground state become almost degenerate, as shown in the left-lower inset of Fig. 3 (b1). In the weak interaction (coupling) regime, the system is in the paramagnetic regime (normal phase) and it goes cross to the ferromagnetic phase at the strong interaction (coupling) regime as $J > J_c$. This phase transition is more clearly seen by the second derivative of the ground state energy shown in Fig.3 (a2) as heavy black solid line. It is more interesting to check this phase transition by its pattern components.

We firstly discuss the ground state shown in Fig. 3 (a1) & (a2). (i) At $J = 0$, the patterns in the same group are degenerate, in which the transverse field leading to quantum fluctuations here determines only the phases in each site, the in-phase of the $i\hat{\sigma}_i^y$ and $\hat{\sigma}_i^z$ has a lower energy and the out-of-phase of them has a higher energy. (ii) With increasing J , the degeneracies are lifted. In the group of lower energy the pattern λ_1 separates itself rapidly from the other patterns by rapidly decreasing of its energy, shown as thin red solid line in Fig. 2 (a1). The energy contributions of the other patterns in this group become more and more less, even the patterns $\lambda_{2,3}$ have a slight increasing at the beginning, but turn back once J approaches to its critical point. (iii) In the group of

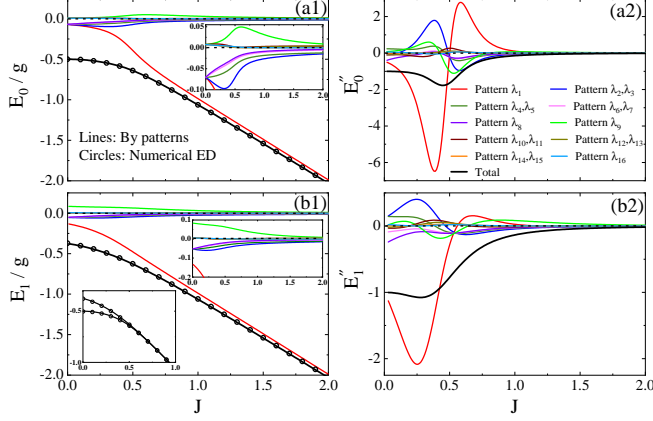


FIG. 3. (a1) & (b1) The energy levels of the ground state and the first excited state as functions of the Ising interaction J , respectively, obtained by Eq. (4) (heavy black solid lines) and the numerical exact diagonalization (circles), which confirms the validity of the pattern picture. In addition, the energy components of the patterns (thin colored solid lines) are also presented and the insets show the details of the patterns except for the pattern λ_1 . (a2) & (b2) The second-order derivatives of the corresponding energy levels (heavy black solid lines) and their pattern components (thin colored solid lines).

higher energy the pattern λ_9 has an apparent response to the change of the interacting strength, and the responses of other patterns in this group keep negligible. (iv) As J goes across the critical point, the energy contributions of all patterns except for the pattern λ_1 become more and more less, and thus the pattern λ_1 dominates. It is not surprising since the pattern λ_1 has a character of long-range ferromagnetic order, which corresponds to the ferromagnetic ground state of the system.

From the above observations, one can clearly see why and how happens the QPT: for $J = 0$ or small J at a given transverse field, various patterns exist and the directions of spins are random, the system is in the paramagnetic phase; as J increases, the order is built gradually by firstly removing the kinks through building the in-phase state of intersites, thus merging the domains, which can be seen from the inset in Fig. 3 (a1). The energy contribution of the patterns $\lambda_{2,3}$ increase at the beginning and then decrease, and the decrease of the energy contribution of the patterns $\lambda_{4,5}$ is not so rapid in comparison to that of the patterns $\lambda_{6,7}$ and λ_8 , where the latter has more domains and kinks and their energy contributions decrease directly in a monotonic way. By the same reason, the domains and kinks involved in the patterns $\lambda_{4,5}$ and $\lambda_{2,3}$ are also further merged or removed by further increasing J up to the J_c , and thus marking the finishing of the phase transition. It is more interesting to check the behavior of the pattern λ_9 , which has a character of in-phase of intersites, but within site the

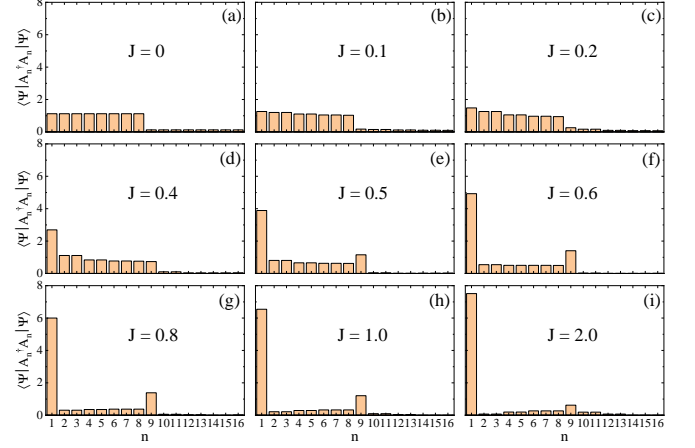


FIG. 4. Histogram of patterns' occupancy in the ground state of the system with $L = 8$ for different Ising interactions $J = 0, 0.1, 0.2, 0.4, 0.5, 0.6, 0.8, 1.0$, and 2.0 , which correspond successively to (a) to (i). The QPT happens around $J = 0.5$.

two operators of $i\hat{\sigma}_i^y$ and $\hat{\sigma}_i^z$ are out-of-phase. It is noticed that after the phases of intersites have been built up, namely, the long-range order forms, the in-phase in each site just begins to form gradually and it lasts in a large interacting strength range, as shown in the inset of Fig. 3 (a1) marked by green line. It is the essential role played by quantum fluctuations, uncovered quantitatively for the first time by identifying explicitly the corresponding pattern.

In order to further emphasize the roles played by the different patterns, we check the second derivatives of the energies contributed by different patterns, as shown in Fig. 3 (a2), from which and the above analysis the patterns λ_1 , $\lambda_{2,3}$, and λ_9 play key roles in the response to the change of the interacting strength: the pattern λ_1 is active since it gains energy with increasing the interacting strength and it drives the happening of the phase transition; the pattern λ_9 is sensitive to the change of the state of the system since its long-range nature of the phase of intersites. In this sense, it plays a role of inspector, which wakens up the other patterns such as the patterns $\lambda_{2,3}$ beginning to respond to the change of the system. Finally, those like patterns $\lambda_{2,3}$ as mediators to stabilize the newly developed phase, namely, the ferromagnetic phase, contributed mainly by the pattern λ_1 . The identifying of roles played by the different patterns in the process of phase transition is our main meaning of dissecting quantum phase transition, as emphasized in the title. A similar analysis is also made for the first excited state, but there the changes are somehow smooth in comparison to the situations of the ground state, as shown in Fig. 3 (b1) & (b2). For simplicity, we do not repeat it in details.

It is useful to check histogram of the patterns' occu-

pancy calculated by $\langle \Psi | \hat{A}_n^\dagger \hat{A}_n | \Psi \rangle$ where $|\Psi\rangle$ is the ground state, as shown in Fig. 4. For a given transverse field, with increasing J it is obvious that the occupancies of the negative energy patterns transfer to the pattern λ_1 and those of the positive energy patterns first transfer to the pattern λ_9 , the lowest energy pattern in the positive energy sector. Upon further increasing the interaction to $J \sim 0.6$ where the phase transition is already finished, the occupancy in the pattern λ_9 begins to decay. At the same time, the other lower energy patterns in the positive energy sector have a slight increasing occupancy, which is obviously due to the quantum fluctuations. This interesting observation should be experimentally tested in quantum spin simulators such as the ion-trap [28].

Summary and Discussion.—We provide a pattern picture obtained by performing successively two diagonalizations to analyze well-studied QPT in the transverse-field Ising model. The patterns consist of single-body lattice operators weighted by pattern wavefunctions obtained by the first diagonalization. Through the analysis of the energy contributions of the different patterns to the ground state and the first excited state obtained by the second diagonalization, it is shown that different patterns play different roles in the process of the QPT from the paramagnetic phase in the weak interaction regime to the ferromagnetic phase in the strong interaction regime. The histogram of the patterns' occupancy with different Ising interactions further uncovers in an intuitive way why and how the QPT takes place.

Although the present work is limited to small lattice size, it has practical interest on quantum simulations [26], which can be applied to test our pattern picture, characterizing the energy competitions between different patterns and their roles in the process of the QPT. Extensions to higher dimensions and other models involving phase transitions and comparison with the conventional formulations of phase transitions are left for future works.

Acknowledgments.—The work is partly supported by the National Key Research and Development Program of China (Grant No. 2022YFA1402704) and the programs for NSFC of China (Grant No. 11834005, Grant No. 12047501).

* luohg@lzu.edu.cn

- [1] L. D. Landau, On the theory of phase transitions. i., Phys. Z. Sowjet. **11** (1937).
- [2] L. D. Landau and E. M. Lifshitz, *Course of Theoretical Physics Vol. 5 Statistical Physics Part I & II 3rd ed.* (Elsevier Ltd., Amsterdam, 1980).
- [3] K. G. Wilson and J. Kogut, The renormalization group and the ϵ expansion, Phys. Rep. **12**, 75 (1974).
- [4] P. M. Chaikin and T. C. Lubensky, *Principles of Condensed Matter Physics* (Cambridge University Press, 2000).
- [5] M. Kastner, Phase transitions and configuration space topology, Rev. Mod. Phys. **80**, 167 (2008).
- [6] C. N. Yang and T. D. Lee, Statistical theory of equations of state and phase transitions. i. theory of condensation, Phys. Rev. **87**, 404 (1952).
- [7] T. W. B. Kibble, Topology of cosmic domains and strings, Journal of Physics A: Mathematical and General **9**, 1387 (1976).
- [8] W. Zurek, Cosmological experiments in superfluid helium?, Nature **317**, 505 (1985).
- [9] W. Zurek, Cosmological experiments in condensed matter systems, Physics Reports **276**, 177 (1996).
- [10] C. N. Weiler, T. W. Neely, D. R. Scherer, A. S. Bradley, M. J. Davis, and B. P. Anderson, Spontaneous vortices in the formation of bose-einstein condensates, Nature **455**, 948 (2008).
- [11] K. Pyka, J. Keller, H. L. Partner, R. Nigmatullin, T. Burgermeister, D. M. Meier, K. Kuhlmann, A. Retzker, M. B. Plenio, W. H. Zurek, A. del Campo, and T. E. Mehlstäubler, Topological defect formation and spontaneous symmetry breaking in ion coulomb crystals, Nature Communications **4**, 2291 (2013).
- [12] S. Deutschländer, P. Dillmann, G. Maret, and P. Keim, Kibble-zurek mechanism in colloidal monolayers, Proceedings of the National Academy of Sciences **112**, 6925 (2015).
- [13] A. Keesling, A. Omran, H. Levine, H. Bernien, H. Pichler, S. Choi, R. Samajdar, S. Schwartz, P. Silvi, S. Sachdev, P. Zoller, M. Endres, M. Greiner, V. Vuletić, and M. D. Lukin, Quantum kibble-zurek mechanism and critical dynamics on a programmable rydberg simulator, Nature **568**, 207 (2019).
- [14] B. Ko, J. W. Park, and Y. Shin, Kibble-zurek universality in a strongly interacting fermi superfluid, Nature Physics **15**, 1227 (2019).
- [15] M. Schmitt, M. M. Rams, J. Dziarmaga, M. Heyl, and W. H. Zurek, Quantum phase transition dynamics in the two-dimensional transverse-field ising model, Science Advances **8**, eabl6850 (2022).
- [16] S. Braun, M. Friesdorf, S. S. Hodgman, M. Schreiber, J. P. Ronzheimer, A. Riera, M. del Rey, I. Bloch, J. Eisert, and U. Schneider, Emergence of coherence and the dynamics of quantum phase transitions, Proceedings of the National Academy of Sciences **112**, 3641 (2015).
- [17] Y.-T. Yang and H.-G. Luo, Dissecting superradiant phase transition in the quantum rabi model, arXiv: 2212.05186 [quant-ph] (2022).
- [18] S. Sachdev, *Quantum phase transitions*, second ed. ed. (Cambridge University Press, Cambridge, 2011).
- [19] A. Dutta, G. Aeppli, B. K. Chakrabarti, U. Divakaran, T. F. Rosenbaum, and D. Sen, in *Quantum Phase Transitions in Transverse Field Spin Models: From Statistical Physics to Quantum Information* (Cambridge University Press, 2015).
- [20] R. Coldea, D. A. Tennant, E. M. Wheeler, E. Wawrzynska, D. Prabhakaran, M. Telling, K. Habicht, P. Smeibidl, and K. Kiefer, Quantum criticality in an ising chain: Experimental evidence for emergent e_8 symmetry, Science **327**, 177 (2010).
- [21] O. Breunig, M. Garst, A. Klümper, J. Rohrkamp, M. M. Turnbull, and T. Lorenz, Quantum criticality in the spin-1/2 heisenberg chain system copper pyrazine dinitrate, Science Advances **3**, eaao3773 (2017).
- [22] A. Friedenauer, H. Schmitz, J. T. Glueckert, D. Por-

- ras, and T. Schaetz, Simulating a quantum magnet with trapped ions, *Nature Physics* **4**, 757 (2008).
- [23] R. Islam, E. Edwards, K. Kim, S. Korenblit, C. Noh, H. Carmichael, G.-D. Lin, L.-M. Duan, C.-C. Joseph Wang, J. Freericks, and C. Monroe, Onset of a quantum phase transition with a trapped ion quantum simulator, *Nature Communications* **2**, 377 (2011).
- [24] K. Kim, S. Korenblit, R. Islam, E. E. Edwards, M.-S. Chang, C. Noh, H. Carmichael, G.-D. Lin, L.-M. Duan, C. C. J. Wang, J. K. Freericks, and C. Monroe, Quantum simulation of the transverse ising model with trapped ions, *New Journal of Physics* **13**, 105003 (2011).
- [25] M. W. Johnson, M. H. S. Amin, S. Gildert, T. Lanting, F. Hamze, N. Dickson, R. Harris, A. J. Berkley, J. Johansson, P. Bunyk, E. M. Chapple, C. Enderud, J. P. Hilton, K. Karimi, E. Ladizinsky, N. Ladizinsky, T. Oh, I. Perminov, C. Rich, M. C. Thom, E. Tolkacheva, C. J. S. Truncik, S. Uchaikin, J. Wang, B. Wilson, and G. Rose, Quantum annealing with manufactured spins, *Nature* **473**, 194 (2011).
- [26] I. M. Georgescu, S. Ashhab, and F. Nori, Quantum simulation, *Rev. Mod. Phys.* **86**, 153 (2014).
- [27] A. Kandala, A. Mezzacapo, K. Temme, M. Takita, M. Brink, J. M. Chow, and J. M. Gambetta, Hardware-efficient variational quantum eigensolver for small molecules and quantum magnets, *Nature* **549**, 242 (2017).
- [28] C. Monroe, W. C. Campbell, L.-M. Duan, Z.-X. Gong, A. V. Gorshkov, P. W. Hess, R. Islam, K. Kim, N. M. Linke, G. Pagano, P. Richerme, C. Senko, and N. Y. Yao, Programmable quantum simulations of spin systems with trapped ions, *Rev. Mod. Phys.* **93**, 025001 (2021).
- [29] Y.-T. Yang and H.-G. Luo, Characterizing superradiant phase in the quantum rabi model, arXiv: 2207.13285 [quant-ph] (2022).